

Vision-Based Navigation using Map Relative Localization for Crewed Lunar Landing Missions

Jonathan Boyd* and Abhinav Kamath*,†

*Department of Mechanical & Aerospace Engineering, University of California, Davis, CA 95616

†Center for Human/Robotics/Vehicle Integration and Performance, University of California, Davis, CA 95616

Abstract—With human missions to the Moon on the horizon, technology used to navigate and land safely is of critical importance. This paper reviews the state-of-the-art for terrain relative navigation (TRN) and its implementation on lunar landers. We propose a simulation of a lunar lander that employs map relative localization to achieve terrain relative navigation. This simulation will be then used to test the sensitivity of position-estimation to variation in the number of features on the lunar surface. This positional error will then be evaluated in terms of the total fuel consumption to reach the target landing location.

Index Terms—lunar lander, terrain relative navigation, map relative localization, visual-odometry, egomotion, fuel-optimal guidance

I. INTRODUCTION

Ever since the Apollo missions, mankind has dreamed of returning to the Moon. The dream might become a reality in the near future with human lunar landing missions on the horizon. The new opportunity to put humans on the Moon presents the same problem that was faced by the Apollo missions - to accurately navigate in a GPS-denied environment. The Apollo missions relied on inertial measurement units (IMU) for approximate localization, and extremely skilled pilots to get the spacecraft to the landing site. Modern technology allows the implementation of more accurate navigation and autonomous landing strategies. The Altair Lunar Lander developed by NASA JPL in 2010, serves as a good example for potential sensors and systems on future landers.

Figure 1 shows that future landers will have far more sensors than just an IMU. The need for additional sensors arises from the fact that IMUs measure acceleration to estimate position. The measured acceleration is integrated twice to obtain position estimates, causing the error in estimation to grow quadratically. Employing a vision-based approach to navigation would help increase the accuracy of position estimation. Since terrain relative navigation (TRN) using visual-odometry measures the position directly, the growth in error is linear, as opposed to quadratic.

There are numerous other methods for implementing improved navigation, but the focus of this paper will be terrain relative navigation (TRN), implemented using a modified version of NASA JPL's Lander Vision System (LVS) that has been developed for the Mars 2020 mission. This system implements a monocular vision system with a Doppler Radar. The Doppler Radar is used for altimetry, while the monocular

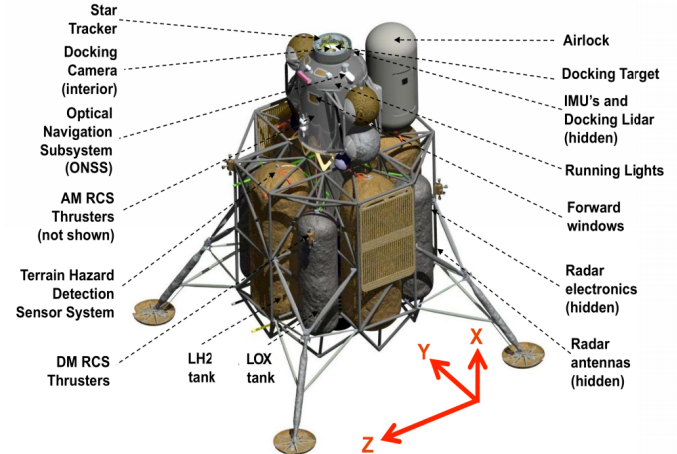


Fig. 1. Systems on the Altair Lunar Lander [1]

vision system is used for egomotion, which is a method for computing the 3D motion of a camera within an environment [2]. The IMU and Radar can be used to seed the vision-based localization algorithm with the approximate initial position. A simulated vision system will be used to evaluate the impact of features on the lunar surface detected by the system on the accuracy of localization.

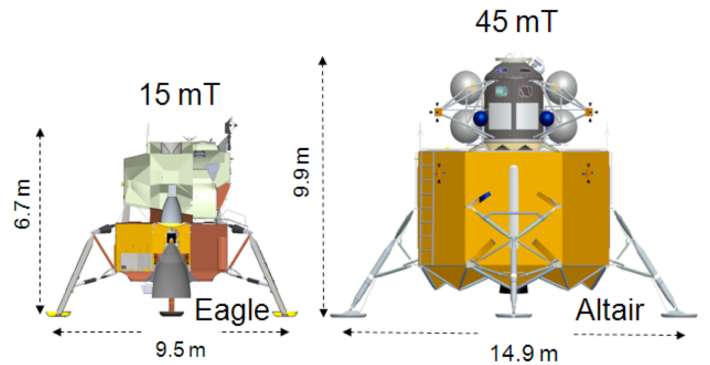


Fig. 2. The Apollo Eagle Lunar Lander & The Altair Lunar Lander [1]

II. LITERATURE REVIEW

For our research question, we investigated localization sensors and algorithms to match the requirements of our chosen lunar lander vehicle model and mission.

A. Localization Sensor Selection

Before the JPL monocular vision system was selected for this simulation, other egomotion strategies were reviewed. The starting point was IMU-only position estimation using dead-reckoning. This method is beneficial because it uses no additional sensors and calculations are simple and quick. Acceleration is simply integrated twice to get position, which results in a quadratically growing error in position estimation. To put this into perspective, the initial position estimation error for the Mars 2020 mission is expected to be 3.2 km before the vision system is used to remove this error [3]. This error leads to extremely large landing ellipses which are not suitable for robotic or human spaceflight missions that require precision landing. Figure 3 shows the landing ellipses of Mars missions, to demonstrate the impact of errors in position estimation.

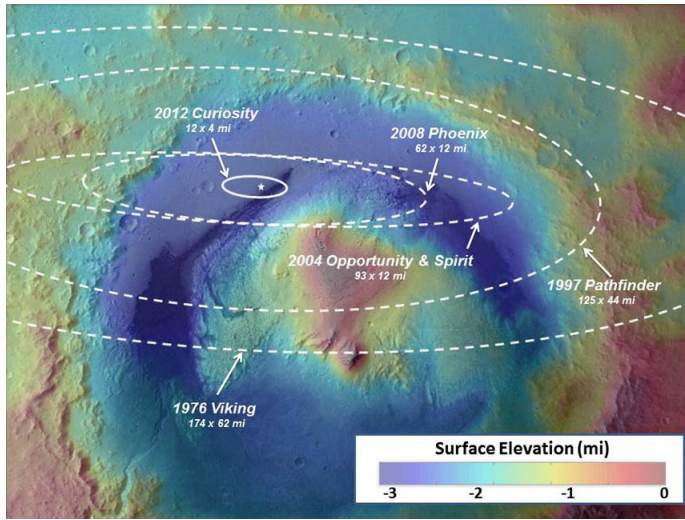


Fig. 3. Landing ellipses of Mars missions [4]

The next intuitive solution is the use of GPS; however, this requires a vast network of satellites in orbit around the celestial body that the mission is exploring. There are no plans to establish such a network around the Moon in the near future. This makes the Moon a GPS-denied environment. Although there is no GPS network on the Moon, extensive lunar surface imaging and mapping are available from orbiters, such as the Lunar Reconnaissance Orbiter (LRO) [5]. This points to a TRN based solution to localization because extensive feature databases and global maps can be generated prior to landing. The engineers behind the Altair Lunar Lander reached a similar conclusion, and a CAD model of the proposed optical navigation sensor is shown in figure 4.

Once a TRN approach to egomotion has been selected, it is necessary to select the appropriate sensor package to implement. The decision comes down to either an active range sensor or a passive image sensor [6]. The active range sensor being considered is a 2D or 3D LIDAR system. The LIDAR benefits from robustness to illumination conditions to the point where it can be used with no light source. The main drawbacks of the LIDAR system are maturity, packaging and power consumption. Compared to a camera sensor, LIDAR is a less

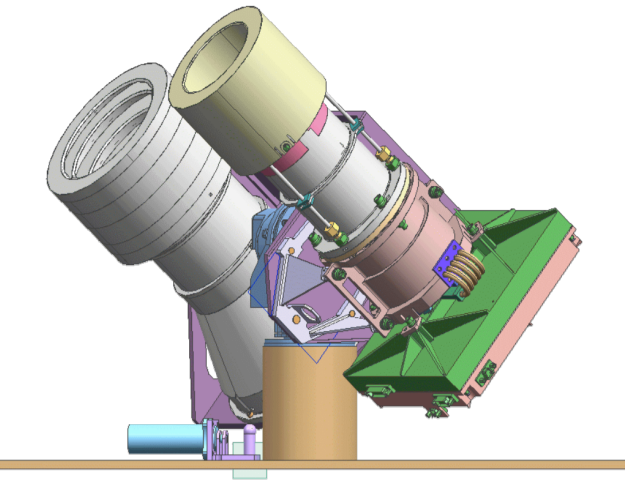


Fig. 4. Altair Optical Navigation Sensor System [1]

mature technology, and currently no LIDAR systems are rated at a technology readiness level (TRL) of nine for space travel [4]. Nine is the highest rating, and it means that the technology is flight proven. In contrast, LIDAR systems are only rated to a maximum TRL level of four. This means that LIDAR systems have only been tested in laboratory settings. A LIDAR system is also larger and heavier than a camera sensor. This large mass increases the cost of launch significantly. In addition, LIDARs also consume more power.

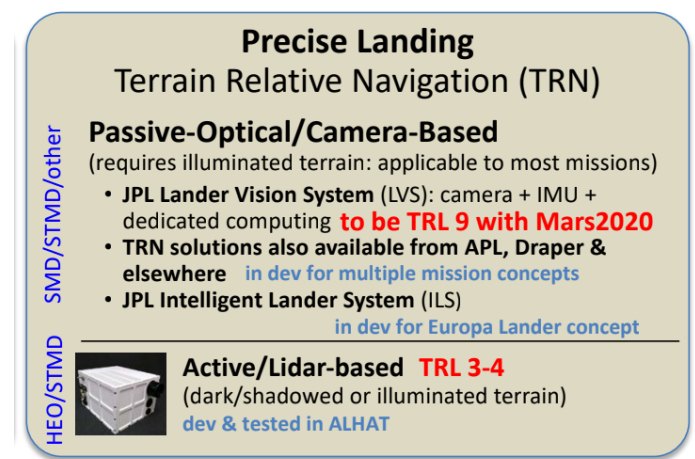


Fig. 5. Current sensor systems that NASA employs for TRN [4]

The main downside of a camera based system is the need for illumination. This constraint does not affect our chosen application because all proposed manned missions to the Moon in the near future involve landing on the near side of the Moon. The impact of varied illumination intensity can also be mitigated by using advanced localization algorithms. Therefore, a camera based system was chosen for this project. Specifically, a monocular camera was chosen, in order to lower the mass of the system. The use of a monocular camera sensor does introduce a scaling problem as the camera system cannot

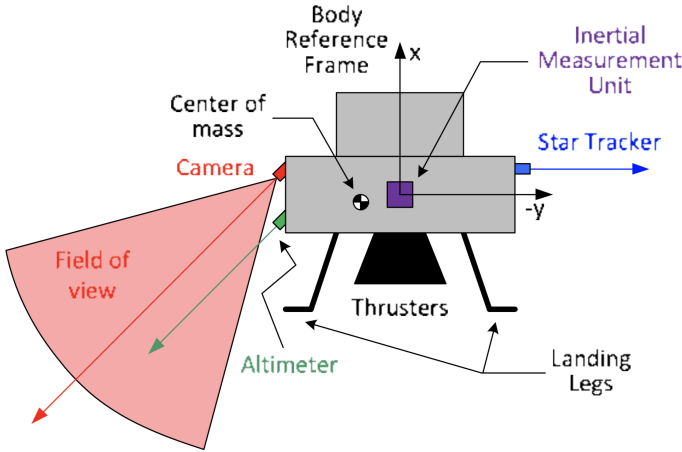


Fig. 6. Sensor placement on a generic lunar landing vehicle [7]

distinguish a far away large object from an up close smaller object. This problem can be addressed with either an additional sensor for altimetry or the use of databases to encode scale information into the global map.

B. Localization Algorithm Selection

Once a camera-based system has been chosen, it is necessary to choose an algorithm to process the captured image for visual-odometry. Image processing algorithms fall into two categories: algorithms to estimate position and attitude, and algorithms to estimate velocity (Table I). Four position estimation algorithms and two velocity estimation algorithms have been investigated. The position estimation algorithms are the *Crater Pattern Matching for Position Estimation (CPMPE)*, the *Scale Invariant Feature Transform (SIFT) Pattern Matching for Position Estimation*, *Onboard Image Reconstruction for Optical Navigation (OBIRON)* - *Surface Patch Correlation for Position Estimation* and *Image to Map Correlation for Position Estimation*. The velocity estimation algorithms are the *Descent Image Motion Estimation Subsystem (DIMES)* - *Consecutive Image Correlation for Velocity Estimation* and *Structure From Motion - Consecutive Image Correlation for Velocity and Attitude Rate Estimation* [6].

Algorithm	Required Inputs	Output Estimate
Crater Pattern Matching	Descent image Crater landmark DB	Absolute position Attitude
SIFT Pattern Matching	Descent image SIFT landmark DB	Absolute position Attitude
OBIRON Surface Patch Correlation	Dense image Descent image Attitude Altitude	Absolute position Attitude update
Image to Map Correlation	Map image Descent image Attitude Altitude	Absolute horizontal position

TABLE I
COMPARISON OF POSITION LOCALIZATION ALGORITHMS [6]

Crater Pattern Matching for Position Estimation was the algorithm chosen for our project. The algorithm works by first creating a crater database from previously collected images of the landing site. The system then compares descent images to this database, in order to determine the global position of the lander. This method can also be used to find the local position by comparing the crater locations in consecutive descent images. The crater pattern matching algorithm is convenient, as it returns position and attitude estimates without the need for additional sensors. It also is robust to varying lighting conditions. This robustness is due to the dark/bright pairing shown in figure 7. The main issue with the algorithm is that it mandates the existence of craters in the vision-field of the camera sensor along the flight path of the lander. This limitation would not be a concern for most lunar missions [8].

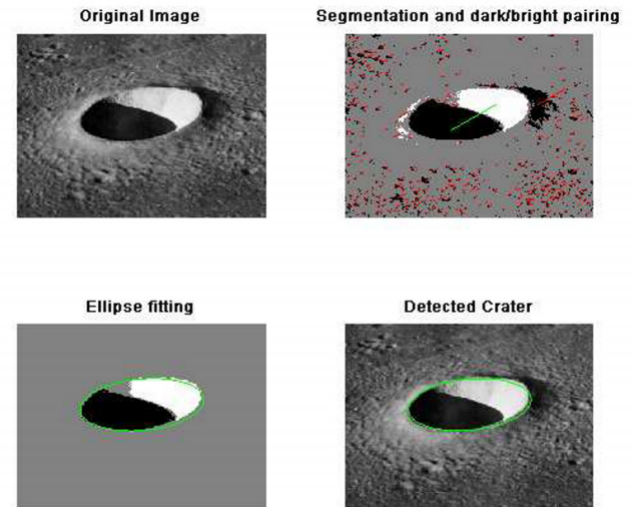


Fig. 7. Steps of crater detection algorithm [9]

Three other algorithms were considered for the project. The first of these algorithms was SIFT Pattern Matching for Position Estimation. It is identical to Crater Pattern Matching except that the features are generalized [10]. This generalization comes at the cost of increased sensitivity to light intensity and view angle. Because the Moon is heavily cratered, the generalized approach is not necessary. Next, OBIRON was investigated. The algorithm uses multiple overlapping orbital images to generate a 3D model of several patches of ground. The 3D models are then used to simulate lighting conditions and generate a simulated image of the ground patch. The descent images are then compared to the simulated image to get position estimates. This method was not selected because it requires altitude and attitude measurements in order to generate the simulated image [11]. The final algorithm considered was Image to Map Correlation for Position Estimation. This method first rectifies the descent image to the same scale and orientation. Then sections of the descent image are compared to the orbital image. This method is currently used on cruise missiles. Map Correlation was not chosen because it requires altitude and attitude information for

image rectification [12], [13].

Although the velocity of the vehicle can be determined by taking multiple position estimates over a known period of time, velocity estimation algorithms provide faster results without the need to reference the global map or feature database. This is done by comparing consecutive images and converting the image-shift to velocity. Although it is likely that we will consider crater matching for consecutive images to determine velocity, we are still working to determine the appropriate velocity estimation algorithm for our purpose. The other two methods previously mentioned have been extensively tested: *DIMES* on Mars rovers and *Structure from Motion* on a helicopter testbed [6].

C. Guidance

Once the position and velocity of the lander are estimated within a range of ‘nominal’ error values, a guidance algorithm is needed to determine the optimal trajectory to the landing site. A multitude of guidance algorithms have been developed to implement fuel-optimal landing. Optimal Control theory has been extensively studied and applied in this regard [14]. The proposed guidance methodology for JPL’s Altair Lunar Lander involved Optimal Control solutions for fuel-efficient trajectory generation [15]. Modern spacecraft landing guidance algorithms rely heavily on Convex Optimization, which ensures a global optimal solution, given that the formulated problem is tractable and that it satisfies a set of well-defined rules [16]. SpaceX uses Convex Optimization in real-time for autonomous precision landing of the first-stage boosters of the Falcon 9 and Falcon Heavy rockets [17]. Engineers at JPL and SpaceX co-developed a real-time implementable fuel-optimal guidance algorithm for planetary pinpoint landing, called the G-FOLD algorithm [18]. As for Earth-based applications, real-time Convex Optimization has been employed to perform constrained motion planning for quadrotors, and this technology is pivotal in being able to operate high-performance aerial robots in populated spaces [19].

III. PROBLEM FORMULATION

A. The Lunar Lander

NASA JPL’s proposed vehicle, the Altair Lunar Lander, will be considered as our model lander.

The lander undocks from the Orion crew capsule in the Low Lunar Orbit (LLO), which is a 100 km circular orbit, and performs the Descent Orbit Insertion (DOI) maneuver. This marks the beginning of the descent phase. This maneuver puts the lander on an elliptical orbit that has a perilune (point on the orbit closest to the lunar surface) of 15.24 km (50,000 ft).

The powered-descent phase of lunar landing commences at this altitude, with the Powered Descent Initiation (PDI), and consists of one continuous, throttled burn, until touchdown [20]. The subphases of powered-descent are as follows:

- 1) The Braking Burn (BB) Maneuver
- 2) The ‘Pitch-Up’ Maneuver

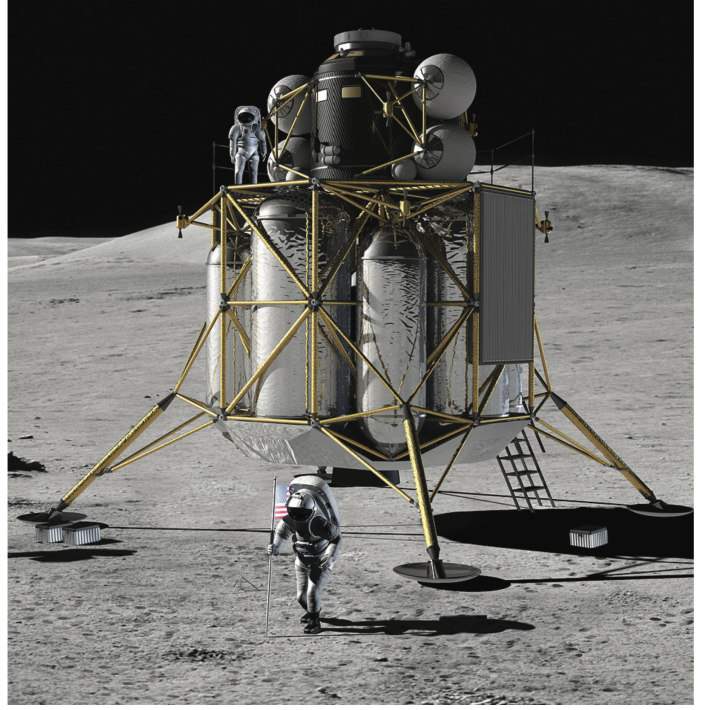


Fig. 8. A depiction of the Altair Lunar Lander on the Moon. Credit:NASA

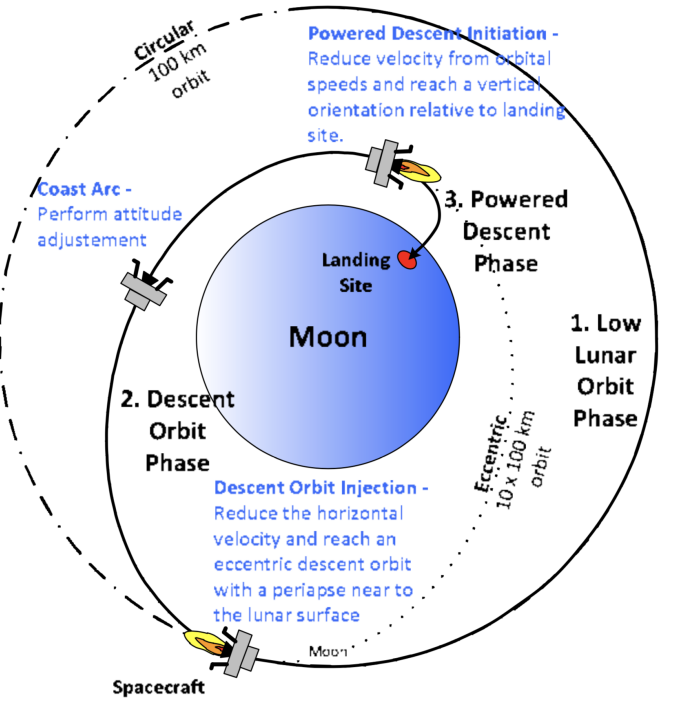


Fig. 9. The phases of lunar descent and landing [7]

- 3) The Approach (visibility) Phase
- 4) The Terminal-Descent (TD) Phase

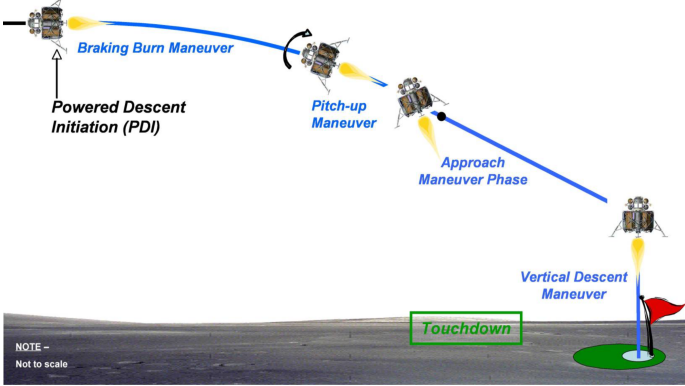


Fig. 10. Lunar Descent Subphases of NASA JPL's Altair Vehicle. [21]

1) *The Braking Burn (BB) Maneuver:* The braking burn is initiated at the perilune of the descent orbit, which is at an altitude of 15.24 km. The main engine is fired at 92% full engine thrust, with the engine aligned with the lander's velocity vector. This thrust margin is required to eliminate potential dispersions during the braking burn.

2) *The 'Pitch-Up' Maneuver:* After completion of the braking burn, the lander commences the 'pitch-up' maneuver to get the lander "nearly vertical". The end of this phase marks the beginning of the approach (visibility) phase.

3) *The Approach (Visibility) Phase:* The engine is fired between 60% and 40% full engine thrust in the approach phase. Redesignation of the target landing site, if required, occurs in this phase. The approach subphase ends at an altitude of 30 meters directly above the final touchdown site, 30 seconds before touchdown.

4) *The Terminal-Descent (TD) Phase:* The TD phase is the final subphase in lunar landing (Fig. 11). It begins at 30 meters directly above the target landing site and continues the burn to get the lander to descend at a constant downward velocity of 1 m/s for the final 30 seconds. This 'vertical-only' descent would help mitigate instability effects relating to fuel-slosh in the tanks. The shutdown sequence is initiated 1 m above the surface to mitigate regolith kick-up at landing.

B. The Human Factor

Safety of the crew is of utmost importance in any human spaceflight mission. This hard requirement on safety drives the design of the lander and the landing trajectory. For example, the 'pitch-up' maneuver is executed at the beginning of the approach phase to provide the crew with better visibility to detect hazards around the landing site, giving them the ability to override the vehicle autonomy at their discretion. This maneuver would involve a change in the attitude of the spacecraft once the landing site enters the field-of-vision of the on-board camera sensor, and this would be encompassed by a 6-DoF guidance algorithm in terms of the numerical requirements [22].

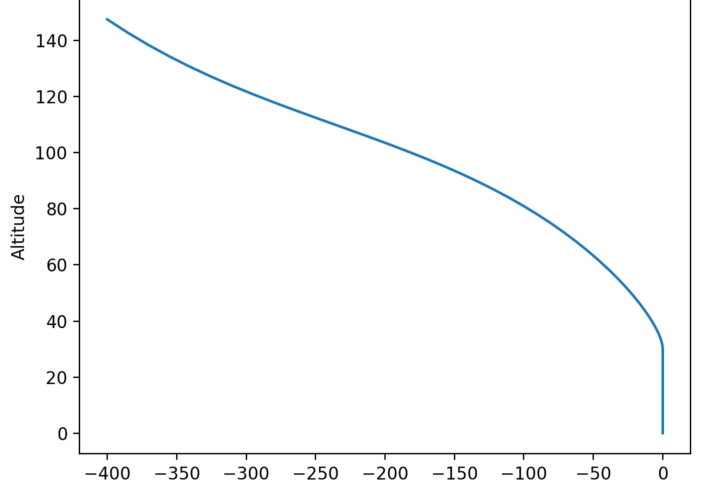


Fig. 11. Fuel-optimal trajectory generated by solving a convex optimization problem, depicting "vertical-only" terminal descent

C. Navigation

We propose a modified version of JPL's Lander Vision System (LVS) for lunar landing missions. As we plan on using a crater-detection algorithm that would use the on-board monocular-vision camera sensor for both localization and altitude estimation, the adopted LVS would not require the Doppler Radar, thus reducing mass and cost.

Navigation of the lunar lander would be based on map relative localization (MRL). This method of localization requires an on-board lunar map. Images captured by the visual-odometry camera sensor would then be matched with the on-board lunar map to get position estimates. With every captured image, the localization error reduces, and the on-board map is cropped accordingly to speed-up computation [3].

We also propose a novel approach to precision landing. The approach would involve storing an image of the landing site along with the on-board map. This would require *a priori* knowledge and selection of the target landing site, which can be made possible by means of an orbiting spacecraft such as the Lunar Reconnaissance Orbiter [5]. For the upcoming Artemis missions, this information can be collected by the Gateway [23].

The Mars 2020 mission will use the Lander Vision System (LVS) for lander state-estimation. The map relative localization (MRL) approach to terrain relative navigation (TRN) begins with a position estimate derived from the on-board IMU. Mars 2020 will begin landing with a parachute phase, and the initial error is estimated to be around 3.2 km [3]. The LVS would then capture a series of six images, the first three for 'coarse' landmark matching and the last three for 'fine' landmark matching. With each image captured and processed, the localization error reduces, and it is estimated to reach a 'nominal' error margin of 40 m after six images, all in a time-frame of 10 seconds.

We presume that localization is performed by the lunar lander until the target landing site is in the field-of-view of the

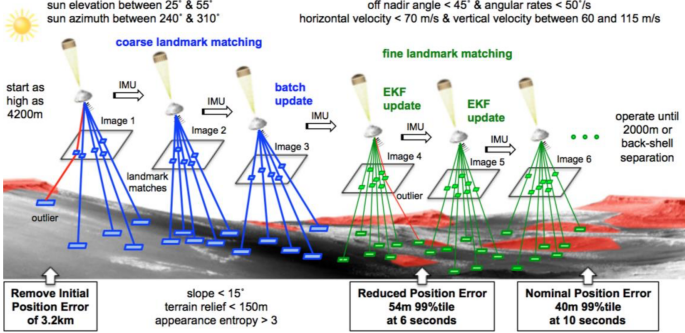


Fig. 12. Map Relative Localization (MRL) on the Mars 2020 lander [3]

on-board camera sensor. The target landing site is detected by using the on-board *a priori* image of the site. At this point, the lander, which is now within a ‘nominal’ range of localization error values, will halt the localization procedure and switch to landing guidance.

D. Guidance

The error in position estimation at the final localization point manifests as the error in the initial position in the landing guidance algorithm. Since the target landing site is now in the field-of-view of the camera sensor, the localization error becomes known to the lander. The fuel-optimal trajectory to the target landing site is generated on-board, and this will inherently correct the positional error of the lander.

E. Objectives

In this project, we propose to develop a simulation to demonstrate vision-based terrain relative navigation (TRN) and fuel-optimal guidance for crewed lunar landing missions. The primary goal of this project is to answer the following questions:

- 1) How does the number of the features of the lunar surface detected by the odometry camera-sensor system affect the localization error?
- 2) How does this position-estimation error that propagates into the lander’s initial position at the beginning of the approach (visibility) phase of lunar landing, affect the total fuel-consumption?

IV. PROPOSED SIMULATION

A. Simulation Environment

1) *Embodiment*: Embodiment of the simulated lander is captured by the physical limitations that are considered, such as its inertial properties and thrust bounds.

2) *Situatedness*: The situatedness of the simulate lander is significant as the camera sensor used for TRN is fixed relative to the spacecraft reference frame. This configuration will be leveraged to estimate the attitude of the lander and will be a consideration during orbital maneuvers, because the camera sensor needs to be facing the lunar surface for TRN to be effective.

3) Assumptions:

- For this project, we consider only the visual-odometry camera sensor for localization, with an initial IMU position seeding
- The lander has one gimbaled main engine thruster, for simplicity of the control architecture.
- The target landing site is assumed to be obstacle-free and safe, as hazard detection and avoidance would involve a reactive control scheme in tandem with the deliberative control scheme, thus making the overall architecture hybrid.
- We assume that the lander tracks the guidance trajectory perfectly for the purposes of this project, as realistic trajectory tracking would involve complex low-level control algorithms.

4) Constraints:

- The main engine can throttle between a minimum and a maximum value of thrust, and this is a limitation of the engine. Once the powered-descent phase commences, a continuous burn is initiated, and the engine cannot be turned off until touchdown. The lower-bound on thrust adds a non-convex constraint in the guidance algorithm. Lossless convexification of this non-convex constraint is needed to make the Convex Optimization problem tractable [24].
- Pointing requirements for the terrain relative navigation sensor add a glide-slope constraint in the guidance algorithm [24].
- The lander is constrained to a ‘vertical-only’ terminal-descent trajectory for the last 30 seconds of landing, in order to avoid instabilities due to fuel slosh and to ensure that the lander does not tip over on touchdown. The engine is turned off 1 meter above the lunar surface to mitigate regolith kick-up. The landing legs are designed to meet this requirement [15].

B. Robotic Architecture

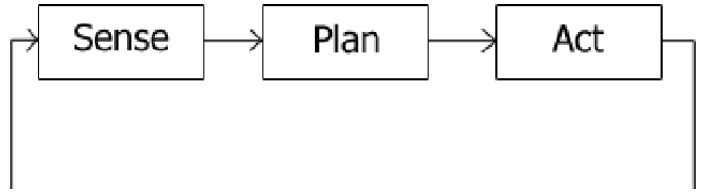


Fig. 13. The Deliberative Control Paradigm [25]

This project will implement a deliberative control architecture:

1) *Sense*: The lander ‘senses’ (estimates) its position using the on-board sensors and map relative localization (MRL). Initial position estimation is subject to IMU drift, which tends to be a large value, and with consequent map relative localization, the estimation error is reduced.

2) *Plan*: After capturing and processing the fixed number of images and detecting the target landing site, the fuel-optimal landing guidance trajectory is generated. This is analogous to robotic path-planning.

3) *Act:* The lander follows the fuel-optimal trajectory by firing its thruster based on the input thrust commands and control system feedback, and lands on the lunar surface.

C. Simulation Framework:

1) *Vision-Based Terrain Relative Navigation:* We will use the Robot Operating System (ROS), which is an open-source robotics middleware for writing robot software, in tandem with a spacecraft simulation environment called SpaceCRAFT VR [26], developed at the AeroSpace, Technology Research and Operations (ASTRO) Center at Texas A&M University, for our simulations. This simulation framework has been used to implement star tracker algorithms in a virtual reality testbed.

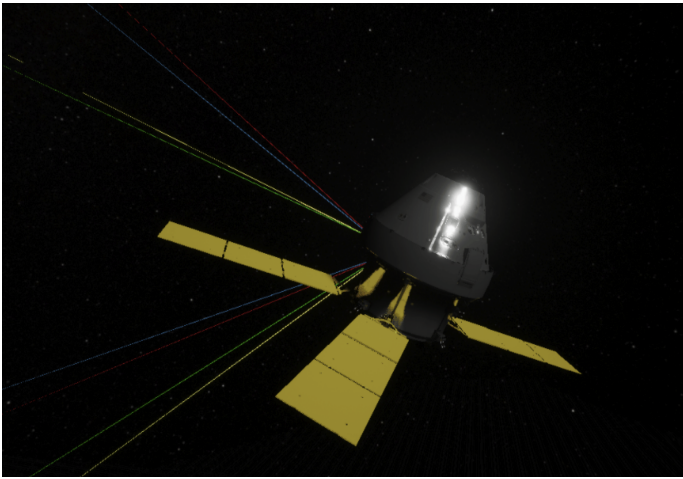


Fig. 14. The Orion Crew Vehicle Represented within SpaceCRAFT VR [27], [26]

2) *Fuel-Optimal Landing Guidance:* We will use the CVXPY framework in Python to generate fuel-optimal landing trajectories subject to all the required constraints.

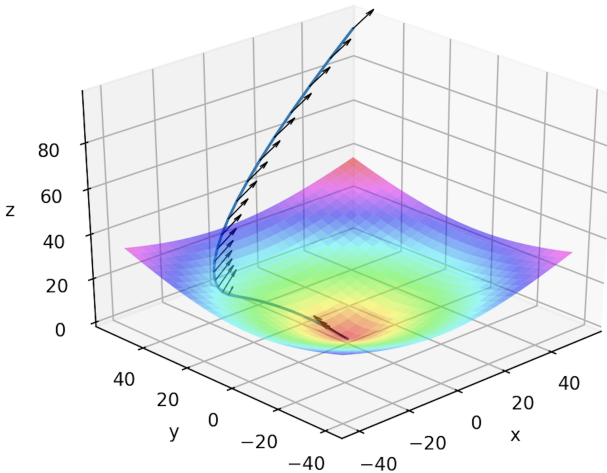


Fig. 15. A sample 3D fuel-optimal landing trajectory generated using CVXPY

V. WORKFLOW TIMELINE

The planned workflow is shown in figure 16. The timeline has been broken down into expected weekly milestones for the remainder of the quarter.

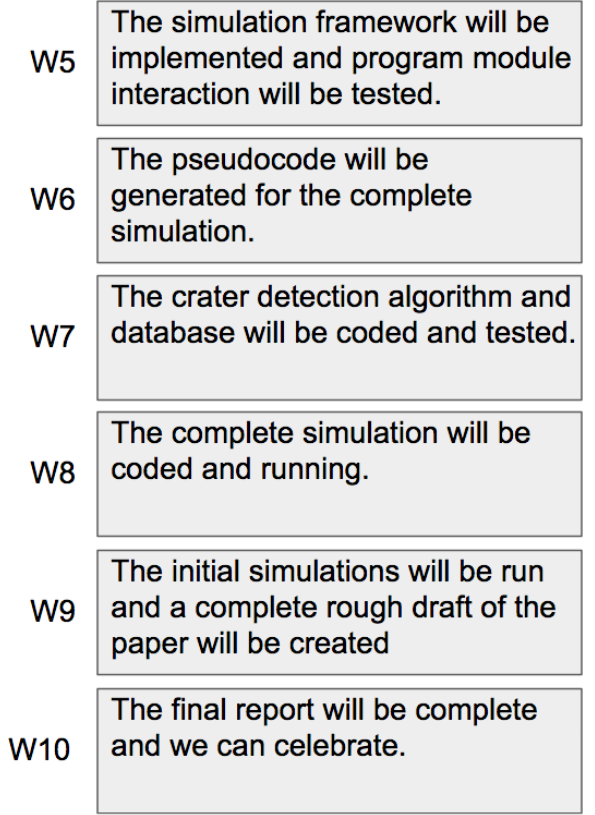


Fig. 16. Project Workflow and Timeline

VI. FUTURE WORK

At the completion of the project, the natural progression of this research project would be to integrate hazard detection and avoidance (HDA) into the simulation environment. This can be executed using the same on-board monocular camera sensor, by implementing obstacle detection algorithms. The simulation can then be augmented to include the final phase of landing with the added obstacle avoidance capability of the lander.

An additional area of interest would be exploring more advanced localization algorithms. Specifically, robustness analysis and implementation of generalized-feature mapping algorithms would enable us to broaden the mission-scope.

REFERENCES

- [1] A. Lee, T. Ely, R. Sostaric, A. Strahan, J. Riedel, M. Ingham, J. Wincentsen, and S. Sarani, "Preliminary design of the guidance, navigation, and control system of the altair lunar lander," in *AIAA Guidance, Navigation, and Control Conference*, 2010, p. 7717.
- [2] M. I. B. Roussos and S. Peleg, "Recovery of ego-motion using image stabilization," 1993.
- [3] A. Johnson, S. Aaron, J. Chang, Y. Cheng, J. Montgomery, S. Mohan, S. Schroeder, B. Tweddle, N. Trawny, and J. Zheng, "The lander vision system for mars 2020 entry descent and landing," 2017.

- [4] C. Restrepo, J. M. Carson III, and M. M. Munk, "Nasa splice project: Development and testing of precision landing gn&cc technologies," 2018.
- [5] R. Vondrak, J. Keller, G. Chin, and J. Garvin, "Lunar reconnaissance orbiter (lro): Observations for lunar exploration and science," *Space science reviews*, vol. 150, no. 1-4, pp. 7–22, 2010.
- [6] A. E. Johnson and J. F. Montgomery, "Overview of terrain relative navigation approaches for precise lunar landing," in *2008 IEEE Aerospace Conference*. IEEE, 2008, pp. 1–10.
- [7] V. S. Bilodeau, S. Clerc, R. Drai, and J. de Lafontaine, "Optical navigation system for pin-point lunar landing," *IFAC Proceedings Volumes*, vol. 47, no. 3, pp. 10 535–10 542, 2014.
- [8] Y. Cheng, A. E. Johnson, L. H. Matthies, and C. F. Olson, "Optical landmark detection for spacecraft navigation," 2003.
- [9] S. Clerc, M. Spigai, and V. Simard-Bilodeau, "A crater detection and identification algorithm for autonomous lunar landing," *IFAC Proceedings Volumes*, vol. 43, no. 16, pp. 527–532, 2010.
- [10] A. Ansar, "small body gn&cc research report: Feature recognition algorithms," *Small Body Guidance Navigation and Control FY 2004 RTD Annual Report (Internal Document)*, pp. 151–171, 2004.
- [11] R. Gaskell, "Automated landmark identification for spacecraft navigation," 2001.
- [12] J. R. Carr and J. S. Sobek, "Digital scene matching area correlator (dsmac)," in *Image Processing For Missile Guidance*, vol. 238. International Society for Optics and Photonics, 1980, pp. 36–41.
- [13] A. Johnson, A. Ansar, L. Matthies, N. Trawny, A. Mourikis, and S. Roumeliotis, "A general approach to terrain relative navigation for planetary landing," in *AIAA Infotech@ Aerospace 2007 Conference and Exhibit*, 2007, p. 2854.
- [14] A. E. Bryson, *Applied optimal control: optimization, estimation and control*. Routledge, 2018.
- [15] A. Lee, "Fuel-efficient descent and landing guidance logic for a safe lunar touchdown," in *AIAA Guidance, Navigation, and Control Conference*, 2011, p. 6499.
- [16] S. Boyd and L. Vandenberghe, *Convex optimization*. Cambridge university press, 2004.
- [17] L. Blackmore, "Autonomous precision landing of space rockets," in *Frontiers of Engineering: Reports on Leading-Edge Engineering from the 2016 Symposium*. National Academies Press, 2017.
- [18] B. Acikmese, J. Casoliva, J. Carson, and L. Blackmore, "G-fold: A real-time implementable fuel optimal large divert guidance algorithm for planetary pinpoint landing," in *Concepts and Approaches for Mars Exploration*, vol. 1679, 2012.
- [19] M. Szmuk, C. A. Pascucci, D. Dueri, and B. Aćikmeşe, "Convexification and real-time on-board optimization for agile quad-rotor maneuvering and obstacle avoidance," in *2017 IEEE/RSJ International Conference on Intelligent Robots and Systems (IROS)*. IEEE, 2017, pp. 4862–4868.
- [20] T. A. Ely, M. Heyne, and J. E. Riedel, "Altair navigation during translunar cruise, lunar orbit, descent, and landing," *Journal of Spacecraft and Rockets*, vol. 49, no. 2, pp. 295–317, 2012.
- [21] L. Kos, T. Polsgrove, R. Sostaric, E. Braden, J. Sullivan, and T. Le, "Altair descent and ascent reference trajectory design and initial dispersion analyses," in *AIAA Guidance, Navigation, and Control Conference*, 2010, p. 7720.
- [22] M. Szmuk, U. Eren, and B. Acikmese, "Successive convexification for mars 6-dof powered descent landing guidance," in *AIAA Guidance, Navigation, and Control Conference*, 2017, p. 1500.
- [23] J. Honeycutt, C. Cianciola, and L. Wooten, "Nasa's space launch system: Artemis 1 vehicle nears completion," 2019.
- [24] J. M. Carson, B. Aćikmeşe, and L. Blackmore, "Lossless convexification of powered-descent guidance with non-convex thrust bound and pointing constraints," in *Proceedings of the 2011 American Control Conference*. IEEE, 2011, pp. 2651–2656.
- [25] "European seventh framework programme fp 7-218086-collaborative project deliverable 2 . 7 proposed algorithms for mission planning for groups of uavs," 2010.
- [26] "SpaceCRAFT VR," www.spacecraft-vr.com.
- [27] N. McHenry, T. Hunt, G. Chamitoff, and D. Mortari, "Virtual reality as a testbed for star tracker algorithms," in *AIAA Scitech 2019 Forum*, 2019, p. 1713.